

Quasi-isochronous experiments with the Super-ACO storage ring

A. Nadji*, P. Brunelle, G. Flynn, M.P. Level, M. Sommer, H. Zyngier

LURE, Université Paris-Sud, 91405 Orsay Cedex, France

Received 28 December 1995

Abstract

The aim of these experiments was to produce short light pulses by reducing the momentum compaction factor. These experiments show that the correction of the second-order term, using sextupole magnets, is essential in order to successfully reduce the momentum compaction by a large factor. By this technique, a factor of 100 reduction was obtained. However, most measurements were performed at a reduction factor of 13. Good agreement was obtained between experimental results and theoretical predictions.

1. Introduction

The natural bunch length and the synchrotron frequency of an electron or positron bunch in a storage ring scale with the square root of the momentum compaction factor α . The reduction of α by a factor of 100 should produce the short natural bunch length of about 10 ps (3 mm) in the case of Super-ACO and 1 ps (0.3 mm) for the case of the SOLEIL project [1].

Such short bunches, if obtained at operational beam current, would lead to an increase in gain for free electron laser operation [2], would be very useful for time resolved experiments, and would provide the possibility of observing coherent radiation [3]. Nevertheless, it is well known that in the turbulent bunch lengthening regime, bunch length becomes independent of α . However, the threshold of this effect depends on the impedance of the machine leaving open the possibility of obtaining high peak currents in future machines by this technique. In addition, it is interesting to study collective beam dynamics at low α as well as to probe the high frequency machine impedance.

When the first-order momentum compaction factor, α_1 , approaches zero, the second order term, α_2 , becomes dominant and must be considered. The longitudinal motion, which includes the momentum compaction factor in its equations, becomes essentially nonlinear. The longitudinal phase-space shape is then modified and the stable region is reduced both in energy and phase. Several theoretical studies have analyzed the second order particle dynamics in a storage ring [4–7] and first experiments to reduce α have been carried out on BESSY I, and on the BNL UV ring [8]. They resulted in a reduction of the

momentum compaction by a factor of 3 and 4 respectively. On UVSOR, Hama et al. have succeeded in obtaining a reduction of a factor 100 with a stored beam current of 0.1 mA at low α [9]. Such experiments are also in progress at the ESRF and ALS storage rings [10,11].

In this paper, we present the method used to obtain variable momentum compaction lattices on Super-ACO, as well as experimental measurements of the first (α_1) and the second (α_2) order terms of the momentum compaction factor. We then describe the operational method allowing to set α_2 to zero and suggest an explanation for the evolution of the beam lifetime during these experiments, using energy acceptance expressions including the term α_2 .

2. Theoretical approach

2.1. Derivation of the momentum compaction factor to second order

The momentum compaction factor is defined as the relative change of the orbit path length, $\Delta l/l_0$, with respect to the relative particle energy deviation, $\Delta p/p_0$:

$$\alpha = \frac{d(\Delta l/l_0)}{d(\Delta p/p_0)} \quad (1)$$

where p_0 is the momentum of the reference particle and l_0 the length of the reference orbit.

Simple geometric considerations lead to the following expression for the change in trajectory length:

$$\frac{\Delta l}{l_0} = \frac{1}{l_0} \int \left[\frac{1}{\cos x'} \left(1 + \frac{x}{\rho_0} \right) - 1 \right] ds, \quad (2)$$

* Corresponding author. Tel. +33 164 468 246, fax +33 164 467497, e-mail: nadji@lure.u-psud.fr.

where ρ_0 is the radius of curvature of the reference orbit and x is the particle amplitude.

By introducing the expression for the particle amplitude composed of betatron oscillation, orbit distortions and off momentum orbits:

$$x = x_\beta + x_{c_0} + \eta_0 \frac{\Delta p}{p_0} + \eta_1 \left(\frac{\Delta p}{p_0} \right)^2 + \dots \quad (3)$$

we can obtain as already demonstrated in Ref. [5], the following expression for $\Delta l/l_0$:

$$\frac{\Delta l}{l_0} = \frac{\Delta \mathcal{C}}{\mathcal{C}} + \alpha_1 \left(\frac{\Delta p}{p_0} \right) + \alpha_2 \left(\frac{\Delta p}{p_0} \right)^2 + \mathcal{O}(3), \quad (4)$$

where

$$\alpha_1 = \frac{1}{l_0} \int \frac{\eta_0}{\rho_0} ds, \quad (5a)$$

$$\alpha_2 = \frac{1}{l_0} \int \left(\frac{\eta_0'^2}{2} + \frac{\eta_1}{\rho_0} \right) ds, \quad (5b)$$

and $\Delta \mathcal{C}/\mathcal{C}$ is the momentum independent term representing lengthening effects due to betatron oscillations and orbit distortions. The effect of the betatron oscillations has been estimated by using the smooth approximation and is found to be small. The closed orbit length depends on the dipole errors and the dispersion at their position. Hence $\Delta \mathcal{C}/\mathcal{C}$ varies during the reduction of α . The term $\Delta \mathcal{C}/\mathcal{C}$ can be cancelled by a change in the RF frequency, $\Delta f_{RF}/f_{RF} = \Delta \mathcal{C}/\mathcal{C}$ permitting to obtain the central RF frequency of the ring.

In Eq. (5), η_0 and η_1 are the first and the second order terms of the dispersion function. Their analytical expressions, given in Ref. [12], show that η_0 depends only on linear optics whereas η_1 also depends on sextupole components. Eq. (5b) shows that, due to the $\eta_0'^2$ contribution, α_2 is always positive in a linear machine. η_1 can be made positive or negative with sextupole and can compensate the term $\eta_0'^2$. The value of α_2 can therefore be controlled and set to zero, allowing for smaller values of α .

We have calculated α_2 for Super-ACO, using Eq. (5b) and checked that it depends linearly on sextupole strength at fixed α_1 .

2.2. Nonlinear longitudinal motion

When α_1 is very small, the second order term α_2 cannot be ignored and must be considered in the equations of longitudinal motion. These nonlinear equations and the higher order Hamiltonian are presented and discussed in Appendix A. They show the existence of a second zone of stability in addition to the well-known stable linear RF-bucket.

This new stable zone is far away from the linear one and thus out of the energy acceptance of the vacuum chamber when α_2 is very small (Fig. 1a). As $|\alpha_2|$ increases, the two

stable buckets approach each other and their separatrices merge for a critical value α_{2c} of α_2 (Fig. 1b), see Appendix A:

$$\alpha_{2c} = \frac{|\alpha_1|}{\sqrt{3} e_{RF}}, \quad (6)$$

where e_{RF} is the bucket half height in the linear case.

For $|\alpha_2| > \alpha_{2c}$, the buckets change their form and the energy and phase acceptances are significantly reduced (Fig. 1c). This leads to a decrease in the Touschek and quantum beam lifetimes. In order to have a small value of α_1 with a good beam lifetime, it is essential to minimize the value of α_2 .

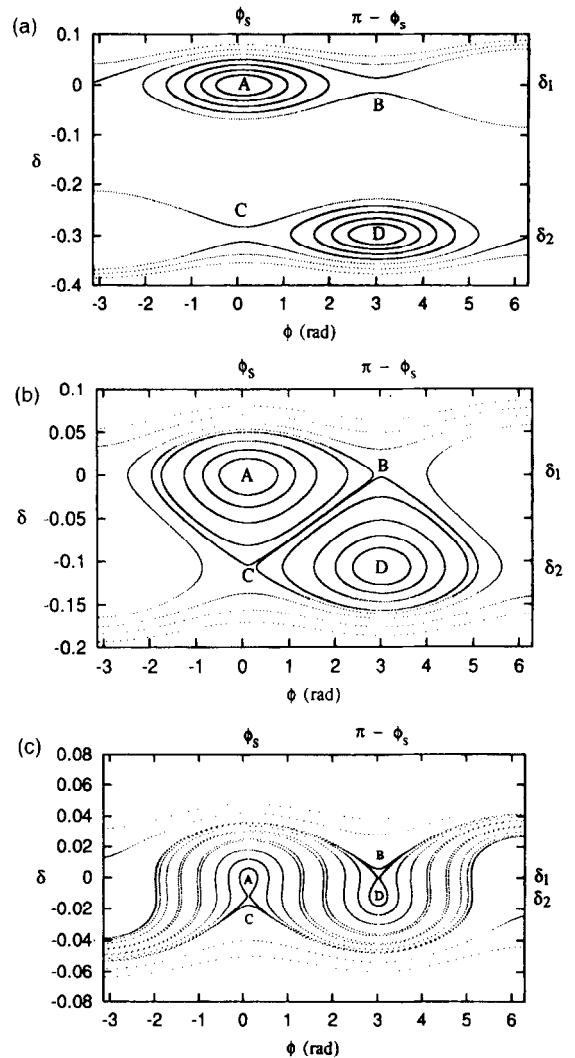


Fig. 1. Longitudinal phase space trajectories for $\phi_s = 0.1256$ rad, $\alpha_1 = 0.00119$. (a) $\alpha_2 = 0.004$, (b) when $\alpha_2 = \alpha_{2c} = 0.011$. (c) when $\alpha_2 \gg \alpha_{2c}$, $\alpha_2 = 0.10$.

3. Quasi-isochronous optics calculation

The standard lattice of Super-ACO is a fourth order symmetry expanded Chasman–Green Double Bend Achromat with four families of quadrupoles and eight straight sections alternately with dispersion (even sections) and without (odd sections). Each quadrupole has extra coils which can be powered to produce a sextupole field. Therefore Super-ACO has four families of sextupoles. The standard Super-ACO lattice ($\varepsilon_s = 37 \text{ nm} \cdot \text{rad}$) does not permit to reach low values of α . That is why, for these experiments, a large emittance detuned optics ($120 \text{ nm} \cdot \text{rad}$) is used, giving an initial α_1 of 0.015 (Fig. 2a).

We used the four families of quadrupoles in order to have η_0 change sign inside the bending magnets. This allows lower values of α and creates negative η_0 in odd sections. Variable momentum compaction lattices were calculated keeping the betatron tunes and the betatron functions nearly constant. Fig. 2b shows the Super-ACO optical functions for a quasi-isochronous operation mode which corresponds to $\alpha_1 = 0.00015$, 100 times smaller than the initial value.

Calculated linear momentum compaction factor values are given in Fig. 3 as a function of the dispersion value η_x^{odd} in odd straight sections. We can see that α_1 decreases

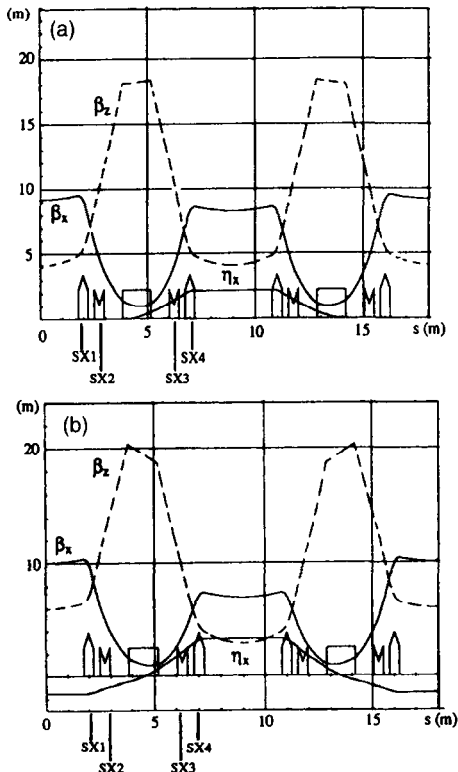


Fig. 2. Super-ACO optical functions for a large emittance detuned optics. (a) $\alpha_1 = 0.015$, (b) $\alpha_1 = 0.00015$.

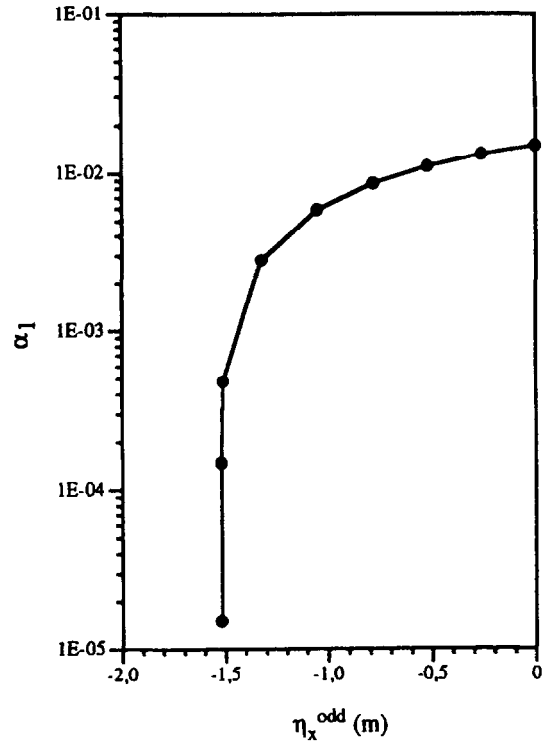


Fig. 3. Variation of calculated α_1 versus η_x in odd straight sections.

slowly from its initial value, down to $\alpha_1 = 0.005$ when η_x^{odd} is changed from 0 to -1 m , then the α_1 value decreases very steeply and changes from $\alpha_1 \approx 0.001$ to $\alpha_1 \approx 0$ between -1.50 and -1.52 m . One should note that the relationship between α_1 and η_x is fairly linear, but since we deal with very low values of α_1 , it is reasonable to plot them on a logarithmic scale. This gives a dramatically steep function which illustrates the sensitivity of α_1 to the quadrupole values.

4. Experimental measurement methods for determining α_1 and α_2

The bunch length scales with the momentum compaction factor α according to

$$\sigma_b = \left(\frac{2\pi hc^2 E_0}{\omega_{RF}^2 \cos \phi_s e V_{RF}} \right)^{1/2} \alpha^{1/2} \sigma_E. \quad (7)$$

However, to obtain α , one has to assume a value for the energy spread σ_E . We therefore choose to use the horizontal closed orbit displacement

$$\Delta x = \eta_x \frac{\Delta p}{p_0} = -\frac{\eta_x}{\alpha} \frac{\Delta f_{RF}}{f_{RF}}, \quad (8)$$

or preferably the synchrotron frequency

$$f_s = f_{REV} \left(\frac{heV_{RF} \cos \phi_s}{2\pi E_0} \right)^{1/2} \alpha^{1/2}, \quad (9)$$

whose measurement is more straightforward and more precise.

Here E_0 is the beam energy, h is the harmonic number, V_{RF} is the RF voltage and ϕ_s the synchronous phase. η_s is the calculated horizontal dispersion at a beam position monitor and $\Delta f_{RF}/f_{RF}$ is the relative change of the RF frequency from the central value.

When α_2 and $\Delta f_{RF}/f_{RF}$ are taken into account, Eqs. (8) and (9) must be recalculated. It is shown in Appendix A that $\Delta p/p_0$ appearing in Eq. (8) is the value which cancels $\Delta l/l_0$ (Eq. 4), and α appearing in Eq. (9) is the derivative of $\Delta l/l_0$.

We shall hence use

$$\frac{\Delta x}{\eta_s} = -\frac{\alpha_1}{2\alpha_2} \left(1 - \sqrt{1 - 4 \frac{\alpha_2}{\alpha_1^2} \frac{\Delta f_{RF}}{f_{RF}}} \right), \quad (10)$$

$$f_s = f_{REV} \sqrt{\frac{heV_{RF} \cos \phi_s}{2\pi E_0} \left(\alpha_1^2 - 4\alpha_2 \frac{\Delta f_{RF}}{f_{RF}} \right)^{1/4}}. \quad (11)$$

Experimental values for α_1 and α_2 can thus be derived by measuring the synchrotron frequency or horizontal beam displacement as a function of RF frequency.

The beam position is measured by monitors (BPM) located between the two quadrupoles of each doublet, with an accuracy of $\pm 10 \mu\text{m}$ and the synchrotron frequency is measured by resonant excitation.

5. Experimental results and discussion

5.1. Measurement of α_1

The quadrupole gradients calculated for each point of the descent path (Fig. 3) were introduced into a control program. The beam was injected at the initial point ($\alpha_1 = 0.015$) and the momentum compaction factor was reduced step by step by changing the quadrupole strengths. This allowed us to study the effects occurring during the process of reducing α . The experiment was performed with a single bunch at the nominal energy of 800 MeV. The peak RF cavity voltage was adjusted to 170 kV.

The synchrotron frequency was measured for each point of the path. In each case, at the operating point corresponding to the calculated value of $\alpha_1 = 0.003$, difficulties occurred in terms of various instabilities, large closed orbit distortion, poor beam lifetime and sudden beam losses. Indeed, at low α , the closed orbit can undergo large distortions for a small deviation of the RF frequency. This distortion is amplified by the large value of the dispersion. The variation of the experimental synchrotron frequency values versus the square root of the calculated α_1 departs from linearity below $\alpha_1 = 0.003$ (Fig. 4). This behaviour is

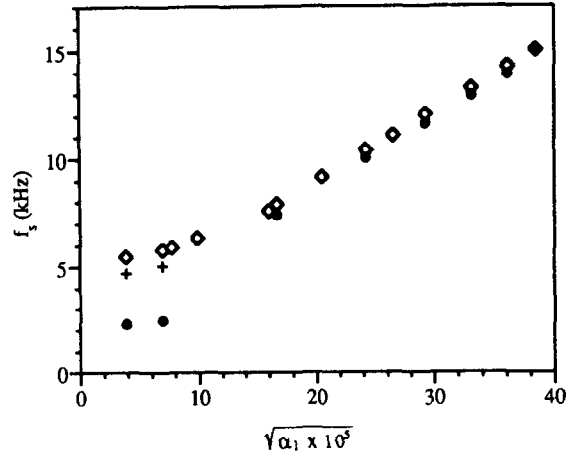


Fig. 4. Measured synchrotron frequency versus calculated α_1 for three different sets of sextupole strengths.

consistent with Eq. (11). The curves of Fig. 4 correspond to three different sets of sextupole strengths. One of these sextupole configurations (dark circles) reduced α_2 to a near-zero value leading to a much lower synchrotron frequency for the same calculated α_1 . At the lowest point, $\alpha_1 = 0.00015$ (100 times smaller than the initial value) the single bunch current was 0.1 mA. This should correspond to a reduction of the natural bunch length by a factor of 10. Unfortunately, the short electrode we use routinely for bunch length measurements does not permit to measure lengths below 50 ps. Therefore no bunch length measurement was done for α_1 smaller than 0.0036 during these experiments.

5.2. Measurement and compensation of α_2

Systematic measurement and control of α_2 were performed for the point corresponding to $\alpha_1 = 0.00119$. The synchrotron frequency was measured as a function of the RF frequency for different strengths of the SX4 focusing sextupole family. Experimental values of α_1 and α_2 were then deduced by fitting Eq. (11). Reducing the SX4 strength by approximately 6% from its nominal value brought the measured α_2 to nearly zero (Fig. 5). At this point, the measured synchrotron frequency was 4.2 kHz which, compared to the 15 kHz synchrotron frequency at the injection point, confirms the reduction of α_1 by a factor 13. The crossing point which is independent of the value of SX4 strength defines the central frequency of the machine.

The variation of α_2 with the SX4 sextupole strength is linear as predicted by the calculation (Fig. 6), and the value of the slope is in good agreement with the calculated one.

The compensation of α_2 at this point of the path allowed us to store 5 mA in a single bunch with corrected chromaticities and beam lifetime longer than 10 h. No

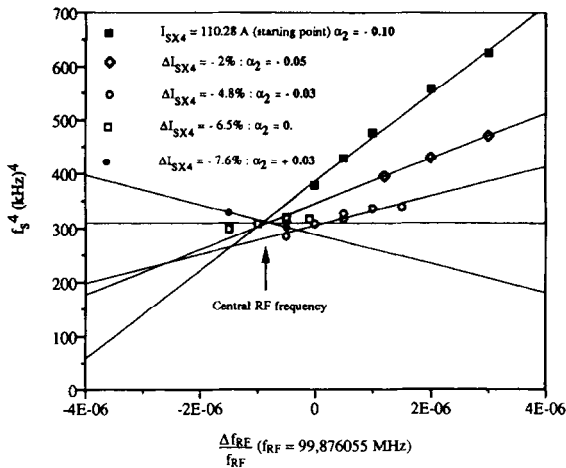


Fig. 5. Variation of the synchrotron frequency versus RF frequency for different sets of sextupoles for $\alpha_1 = 0.00119$.

bunch length measurements were performed for this particular value of α_1 . The turbulent bunch lengthening model predicts no effect of α_1 on bunch length above the threshold. Experimental measurements at $\alpha_1 = 0.015$ and $\alpha_1 = 0.0036$ shown in Fig. 7 are compatible with this theory.

5.3. Values of α_1 and α_2 deduced from orbit variations

The orbit variations were also measured as a function of Δf_{RF} at $\alpha_1 = 0.00119$, using a set of sextupole strengths corresponding to $\alpha_2 = -0.18$ (measured by fitting Eq. (11) at the same point). Fig. 8 shows the variation of $\Delta p/p_0$ deduced from the measurements of Δx (average value over the 16 BPMs) as a function of Δf_{RF} . The experimental points are in good agreement with Eq. (10) calculated for $\alpha_1 = 0.00119$ and $\alpha_2 = -0.18$.

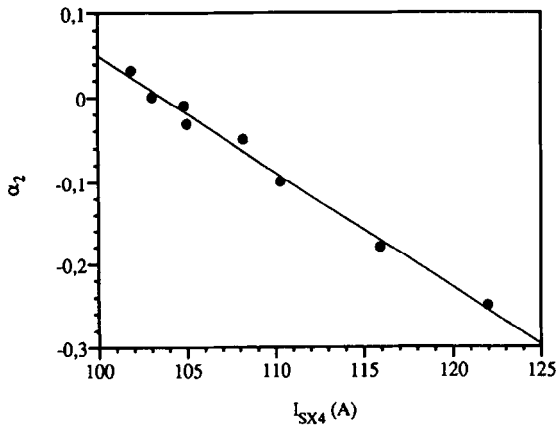


Fig. 6. Variation of α_2 versus sextupole strength SX4 for $\alpha_1 = 0.00119$.

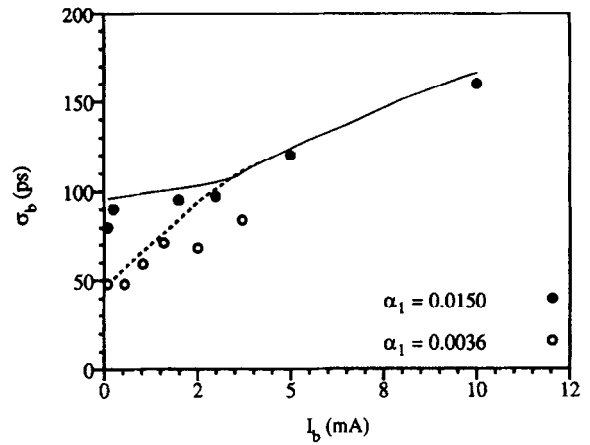


Fig. 7. Bunch lengthening for different values of α_1 .

6. Energy acceptance and beam lifetime

As discussed in Appendix A, when $|\alpha_2| \gg \alpha_{2C}$, the bucket is asymmetric in energy. The energy and phase acceptances in this case are reduced. The bucket height has been calculated as a function of α_2 and $\Delta f_{RF}/f_{RF}$ (see Appendix B) as being:

$$\delta(|\alpha_2| \gg \alpha_{2C}) = \frac{3}{2} \left| \frac{\alpha_1}{\alpha_2} \right| \sqrt{1 - 4 \frac{\alpha_2}{\alpha_1^2} \frac{\Delta f_{RF}}{f_{RF}}} \quad (12)$$

One can notice that when the term $(4\alpha_2/\alpha_1^2)(\Delta f_{RF}/f_{RF})$ approaches unity, the value of δ tends toward zero and the beam lifetime is then significantly reduced.

When α_1 is negative (which was usually the case during this experiment) a reduction of δ is expected when $\Delta f_{RF}/f_{RF}$ is negative. This has been confirmed during these experiments, where a severe decrease in beam lifetime was always observed when both $\Delta f_{RF}/f_{RF}$ and α_2 were nega-

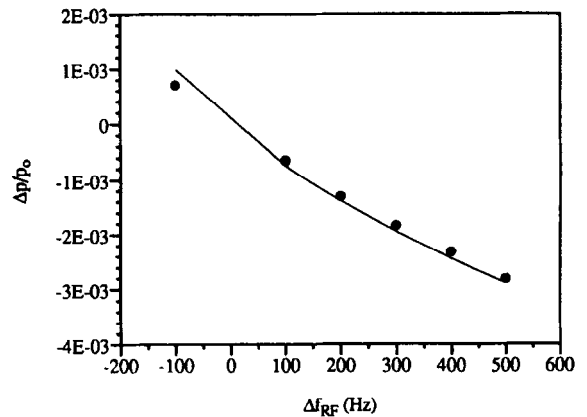


Fig. 8. Variation of $\Delta p/p_0$ versus RF frequency for $\alpha_1 = 0.00119$ and $\alpha_2 = -0.18$.

tive. On the other hand, the measured lifetime was much better when the product $\alpha_2(\Delta f_{\text{RF}}/f_{\text{RF}})$ is negative.

When α_1 is reduced, the sensitivity to the closed orbit errors is enhanced, and it becomes difficult to control the sign of the trajectory length deviation. It is then essential to be able to control α_2 using sextupoles. This, added to the chromaticity control necessitates at least three sextupole families.

7. Conclusion

We have succeeded in reducing α_1 by a factor of 100 by both changing the dispersion function in the bending magnets and compensating the second-order momentum compaction factor α_2 . Systematic measurements were performed at $\alpha_1 = 0.00119$ which represents a reduction by a factor of 13. The term α_2 was successfully set to zero with corrected closed orbit and the two transverse chromaticities compensated simultaneously. In this case we could store a single bunch of 5 mA with greater than 10 h lifetime. The measured synchrotron frequency confirmed this reduction of α_1 .

The bunch length was measured at two values of α_1 , respectively 0.015 and 0.0036 and shows that bunch shortening is only clear at very low current.

In addition, experiments with negative momentum compaction factor are currently being performed in order to test the predictions of beam stability with natural chromaticities and the variations of bunch length and energy spread versus bunch current.

Acknowledgements

We would like to thank L. Cassinari and J. Darpentigny for their collaboration concerning synchrotron frequency and bunch length measurements. We are also indebted to the operations group for their constant assistance. Finally, we would like to thank M.E. Couprie and her team for their participation.

Appendix A. Non-linear synchrotron motion

The synchrotron motion equations to second-order can be written as:

$$\frac{d\varphi}{dt} = -\omega_{\text{RF}} \left[\alpha_1 \delta + \alpha_2 \delta^2 + \frac{\Delta\mathcal{C}}{\mathcal{C}} \right],$$

$$\frac{d\delta}{dt} = \frac{eV_{\text{RF}}}{E_0 T_0} [\sin \varphi - \sin \varphi_s],$$

α_1 and α_2 are respectively the first and second-order momentum compaction factors, $\Delta\mathcal{C}/\mathcal{C}$ is the momentum independent term (cf. Section 2.1), δ is the energy

deviation $\Delta p/p_0$, ω_{RF} is the angular frequency of the RF cavity, V_{RF} is the RF peak voltage, E_0 is the particle energy and T_0 the revolution period, φ_s and φ are respectively the phases of the reference and the arbitrary particles.

These equations can be derived from the Hamiltonian:

$$\mathcal{H}(\delta, \varphi) = -\omega_{\text{RF}} [\mathcal{D}(\delta) - \mathcal{F}(\varphi)],$$

where

$$\mathcal{D}(\delta) = \frac{\Delta\mathcal{C}}{\mathcal{C}} \delta + \alpha_1 \frac{\delta^2}{2} + \alpha_2 \frac{\delta^3}{3},$$

$$\mathcal{F}(\varphi) = \frac{eV_{\text{RF}}}{E_0 T_0} (\cos \varphi - \cos \varphi_s + (\varphi - \varphi_s) \sin \varphi_s).$$

In the usual approximation ($\alpha_2 = 0$), there are two fixed points corresponding to $d\varphi/dt = 0$ and $d\delta/dt = 0$. The fixed point located at $(\varphi = \varphi_s, \delta = 0)$ is stable and the fixed point located at $(\varphi = \pi - \varphi_s, \delta = 0)$ is unstable, when $\alpha_1 > 0$. Around the stable point, the synchrotron frequency is:

$$f_s = f_{\text{REV}} \left(\frac{heV_{\text{RF}} \cos \phi_s}{2\pi E_0} \right)^{1/2} \alpha^{1/2}.$$

In the present case ($\alpha_2 \neq 0$ and $\Delta\mathcal{C}/\mathcal{C} \neq 0$) the requirements $d\varphi/dt = 0$ and $d\delta/dt = 0$, give two stable fixed points and two unstable fixed ones (Fig. 1, cf. Section 2.2). The stable fixed points are (in the case $\alpha_1 > 0$):

$$(\varphi_A = \varphi_s, \delta_A = \delta_1) \quad \text{and} \quad (\varphi_D = \pi - \varphi_s, \delta_D = \delta_2),$$

and the unstable fixed points are:

$$(\varphi_B = \pi - \varphi_s, \delta_B = \delta_1) \quad \text{and} \quad (\varphi_C = \varphi_s, \delta_C = \delta_2),$$

where δ_1 and δ_2 are the solutions of the quadratic equation ($d\delta/dt = 0$), $\alpha_2 \delta^2 + \alpha_1 \delta + \Delta\mathcal{C}/\mathcal{C} = 0$:

$$\delta_{1,2} = \frac{-\alpha_1}{2\alpha_2} \left(1 \pm \sqrt{1 - \frac{4\alpha_2}{\alpha_1^2} \frac{\Delta\mathcal{C}}{\mathcal{C}}} \right).$$

There are now two stable zones and according to α_2 and $\Delta\mathcal{C}/\mathcal{C}$ values, the synchrotron diagram presents three different aspects (Fig. 1, cf. Section 2.2). The synchrotron frequency is the same as before, with $\alpha = \partial(\Delta I/I_0)/\partial\delta = \alpha_1 + 2\alpha_2\delta$, or taking into account the value of δ :

$$\alpha = \pm \alpha_1 \sqrt{1 - \frac{4\alpha_2}{\alpha_1^2} \frac{\Delta\mathcal{C}}{\mathcal{C}}},$$

and

$$f_s = f_{\text{REV}} \sqrt{\frac{heV_{\text{RF}} \cos \phi_s}{2\pi E_0} \left(\alpha_1^2 - 4\alpha_2 \frac{\Delta\mathcal{C}}{\mathcal{C}} \right)^{1/4}}.$$

For $\Delta\mathcal{C}/\mathcal{C} = 0$, one obtains for δ_1 the linear result ($\delta_1 = \delta_A = \delta_B = 0$) and $-\alpha_1/\alpha_2$ for δ_2 . When $\Delta\mathcal{C}/\mathcal{C} \neq 0$, the locations of the fixed points depend on orbit distortions and the amplitude of betatron oscillations. In addition, one

can see a significant reduction in the energy and phase acceptances, due to α_2 and $\Delta\mathcal{C}/\mathcal{C}$ contributions.

Fig. 1b (cf. Section 2.2) represents the transition between the two cases ($|\alpha_2| \ll |\alpha_1|$ and $|\alpha_2| \gg |\alpha_1|$) when the separatrices of the buckets merge and share their unstable fixed points. The Hamiltonian for these fixed points are then equal and one can derive the critical value for α_2 corresponding to the transition by putting:

$$\mathcal{H}_B(\pi - \varphi_s, \delta_B) = \mathcal{H}_C(\varphi_s, \delta_C),$$

which gives after neglecting in this case the term $\Delta\mathcal{C}/\mathcal{C}$:

$$\frac{1}{6} \frac{\alpha_1^3}{\alpha_2^2} - \frac{2 e V_{RF}}{E_0 T_0 \omega_{RF}} \left[\cos \varphi_s + \left(\frac{\pi}{2} - \varphi_s \right) \sin \varphi_s \right] = 0.$$

The critical value for α_2 is then:

$$\alpha_{2c} = \left(\frac{E_0 T_0 \omega_{RF} |\alpha_1^3|}{12 e V_{RF} \left(-\cos \varphi_s + \left(\frac{\pi}{2} - \varphi_s \right) \sin \varphi_s \right)} \right)^{1/2},$$

where we can identify the expression of the bucket half height in the linear case:

$$\varepsilon_{RF} = \left(\frac{2 e V_{RF}}{\alpha_1 E_0 \pi h} \left(-\cos \varphi_s + \left(\frac{\pi}{2} - \varphi_s \right) \sin \varphi_s \right) \right)^{1/2},$$

giving the following simple expression of α_{2c} :

$$\alpha_{2c} = \frac{|\alpha_1|}{\sqrt{3} \varepsilon_{RF}}.$$

Appendix B. Bucket height when $|\alpha_2| \gg \alpha_{2c}$

When $|\alpha_2|$ is greater than α_{2c} , the bucket is asymmetric in energy, and there is no simple definition of the energy acceptance. Therefore, we shall rather speak of the total bucket height (Fig. 1c, cf. Section 2.2).

The extreme points δ and δ_C have the same value of the Hamiltonian (cf. Appendix A), and are related by:

$$\mathcal{H}(\delta, \varphi_s) = \mathcal{H}(\delta_C, \varphi_s),$$

$$(\delta - \delta_C) \left(\alpha_1 \frac{\delta + \delta_C}{2} + \alpha_2 \frac{\delta^2 + \delta \delta_C + \delta_C^2}{3} \right) = 0,$$

taking into account the requirement:

$$\frac{d\delta_C}{dt} = 0 = \alpha_1 \delta_C + \alpha_2 \delta_C^2 + \frac{\Delta f_{RF}}{f_{RF}}$$

(where the relation $\Delta\mathcal{C}/\mathcal{C} = \Delta f_{RF}/f_{RF}$ is used) one can obtain the following equation:

$$(\delta - \delta_C)^2 \left(\frac{\alpha_1}{2} + \alpha_2 \frac{\delta + 2\delta_C}{3} \right) = 0.$$

Two of the three solutions of this equation are the same and represent the momentum at the fixed point C.

The third solution which represents the ordinate of the other extreme point is obtained by setting:

$$\frac{\alpha_1}{2} + \alpha_2 \frac{\delta + 2\delta_C}{3} = 0.$$

We can then deduce the maximum height of the bucket which is equal to:

$$|\delta - \delta_C| = \frac{3}{2} \left| \frac{\alpha_1}{\alpha_2} \right| \sqrt{1 - 4 \frac{\alpha_2}{\alpha_1^2} \frac{\Delta f_{RF}}{f_{RF}}}.$$

References

- [1] M.P. Level et al., IEEE 1995 PAC and ICHEA Conf. Proc., p. 293
- [2] D.A.G. Deacon, Phys. Rep. 76 (1981) 349.
- [3] J.B. Murphy et al., IEEE 1995 PAC and ICHEA Conf. Proc., p. 284
- [4] H. Bruck et al., IEEE Nucl. Sci. (1973) 822.
- [5] H. Wiedemann, SSRL ACD-Note 125, August 1992.
- [6] D. Robin et al., Phys. Rev. E 48 (1993) 2149.
- [7] L. Lin and C.E.T. Gonçalves da Silva, Nucl. Instr. and Meth. A 329 (1993) 9.
- [8] S. Krinsky et al., BNL-46615 (1991).
- [9] H. Hama et al., Nucl. Instr. and Meth. A 329 (1993) 29.
- [10] L. Farvacque et al., Proc. Micro Bunches Workshop, Upton, NY, 1995, AIP Conf. Proc. 367, p. 245.
- [11] D. Robin et al., Proc. Micro Bunches Workshop, Upton, NY, 1995, AIP Conf. Proc. 367, p. 181.
- [12] J.-P. Delahaye and J. Jäger, Part. Accel. 18 (1986) 183.